A&A 393, 33–42 (2002)
DOI: 10.1051/0004-6361:20020925

Astronomy & Astrophysics

Spectral Energy Distributions of starburst galaxies in the 900–1200 Å range

V. Buat[1], D. Burgarella[1], J. M. Deharveng[1], and D. Kunth[2]

[1] Laboratoire d'Astrophysique de Marseille, BP 8, 13376 Marseille Cedex 12, France
e-mail: denis.burgarella@astrsp-mrs.fr,jean-michel.d eharveng@astrsp-mrs.fr
[2] Institut d'Astrophysique de Paris, Bd Arago, Paris, France
e-mail: kunth@iap.fr

Received 21 May 2002 / Accepted 6 June 2002

Abstract. We present the 970–1175 Å spectral energy distributions (SEDs) of 12 starburst galaxies observed with the Far Ultraviolet Spectroscopic Explorer *FUSE*. We benefit from the high spectral resolution of *FUSE* to estimate a continuum as much as possible unaffected by the interstellar lines. The continuum is rather flat with, in a few cases, a decrease at $\lambda < 1050$ Å, the amplitude of which is correlated with various indicators of dust extinction. The far-*UV* SEDs are compared with synthetic population models. The galaxies with almost no extinction have an SED consistent with on-going star formation over some Myrs. We derive a mean dust attenuation law in the wavelength range 965–1140 Å by comparing the SED of obscured galaxies to an empirical dust-free SED. The extinction is nearly constant longward of 1040 Å but rises at shorter wavelengths. We compare our results with other studies of extinction for galaxies and stars in this wavelength range.

Key words. galaxies: starburst – ISM: dust, extinction – ultraviolet: galaxies

1. Introduction

The spectral energy distribution (SED) of star-forming galaxies in the far-*UV* (900–2000 Å) is known to be determined by the stellar initial mass function, the recent star formation history and dust extinction. As a consequence, the far-*UV* observations of galaxies are of fundamental importance to understand the very recent star formation history in the universe and to interpret the spectra of high-z galaxies.

Thanks to the spectral observations of the *IUE* satellite together with wide field *UV* imagers (SCAP (Donas et al. 1987), FOCA (Milliard et al. 1994, UIT (Stecher et al. 1997) or FAUST (Deharveng et al. 1994) experiments), our knowledge of the extinction longward of 1200 Å has considerably improved during the last 10 years. Even though we are far from a complete understanding of the interplay of dust and *UV* emitting sources within galaxies, empirical laws have been found which allow us to estimate the extinction in galaxies, especially in starbursting objects (e.g. Calzetti et al. 2000 and references therein). These successes may be traced back to the fact that the *UV* energy distribution for young starbursts are very similar. They can be fitted by a power-law (Leitherer & Heckman 1995) and changes in the exponent of the power-law can be attributed to reddening (Calzetti et al. 1994; Meurer et al. 1995).

Stellar population models show that these properties slightly change in the 900–1200 Å domain. The time scale for reaching the equilibrium of *UV* flux in constant star formation gets shorter and, alternatively, age effects get more significant for instantaneous bursts. The SED cannot be fitted by a simple power-law, making the potential separation of age and reddening more difficult in practical terms. Observations of the spectral energy distribution of star-forming galaxies downward of 1200 Å have been scarce so far and until recently were limited to those obtained with the Hopkins Ultraviolet Telescope (HUT): 19 spectra have been recently analyzed and an attenuation law for star-forming galaxies derived from 900 to 1800 Å by Leitherer et al. (2002).

FUSE (*Far Ultraviolet Spectroscopic Explorer*) has recently opened access into the 900–1200 Å range and the possibility of observing star-forming galaxies in this domain (e.g. Thuan et al. 2002; Heckman et al. 2001a). Although its very high spectral resolution is suited to the analysis of spectral lines, *FUSE* can also be used to analyse the continuum emission of starburst galaxies in an attempt to study their star formation history and their internal extinction. The high spectral resolution allows better evaluation of the continuum in the presence of numerous absorption features compared to the earlier

Send offprint requests to: V. Buat,
e-mail: veronique.buat@astrsp-mrs.fr

work of Leitherer et al. (2002) with HUT data. In the following, we report such an analysis for a sample of 12 starburst galaxies.

2. Observations and data reduction

2.1. The sample

From June 2000 to December 2001, we obtained spectra from the center of six nearby starburst galaxies with *FUSE* (Guest Investigator Program A023). One object was not retained for analysis but we added data from the *FUSE* archive and built a sample of 12 starburst galaxies appropriate for studying the FUV (900–1200 Å) spectral energy distribution.

The starburst galaxies were primarily selected to cover a range as large as possible in dust extinction. The dust extinction was estimated with both the far-infrared to ultraviolet flux (1600 Å) ratio and the shape of the *UV* continuum longward of 1200 Å. All the targets were detected by *IRAS* and integrated fluxes are available at 60 and 100 μm except for Tol1247-232 which is only detected at 60 μm. The individual fluxes are listed in Table 1. The FIR (40–120 μm) emission was calculated by combining the fluxes at 60 and 100 μm (Helou et al. 1988). In the case of Tol1247-232 we adopted the average value $F_{100}/F_{60} = 1.5$ found for the other galaxies of our sample. Getting a FIR to *UV* flux ratio representative of the central region observed by *FUSE* (30×30 arcsec^2) is an issue since the *IRAS* data are integrated over the galaxies. All the galaxies were observed by *IUE* but were done so through a small diaphragm (10×20 arsec^2). In the case of small galaxies like MRK54, Tol1247-232 or Tol1924-416, the flux at 1600 Å measured by *IUE* can be considered as representative of the total flux emitted by the galaxy and a reliable FIR to *UV* flux ratio can be estimated. Unfortunately most of our galaxies have angular sizes much larger than the *FUSE* and *IUE* apertures. Therefore we compiled integrated *UV* fluxes from the literature which were extrapolated to 1600 Å using the power law $F_\lambda \propto \lambda^\beta$ (Calzetti et al. 1994). For three targets (NGC 3504, NGC 7714, NGC 1140) no complementary *UV* data were found. Nevertheless, because of the moderate size and the high compactness of NGC 7714 and NGC 1140 we used the *IUE* fluxes and the resulting FIR to *UV* flux ratio is taken as an upper limit for these two targets. No FIR to *UV* flux ratio was calculated for NGC 5236: an integrated FIR to *UV* flux ratio for this very large galaxy cannot be representative of the central region observed by *FUSE*.

The cases of NGC 3690 and MRK59 deserve further comment:
NGC 3690 is referred to a galaxy pair in the NASA/IPAC Extragalactic Database (NED), NGC 3690 and IC694 form the Galaxy Triplet Arp299: the *FUSE* aperture is centered on the first galaxy of the pair referenced as NGC 3690 NED1 in (NED) whereas *IUE* observed the central position of the pair. Meurer et al. (1995) found a larger flux with *HST*/FOC at the same position as *IUE* and concluded that the *IUE* aperture was not centered on NGC 3690. Therefore we adopted the total flux of *HST*/FOC and the slope of the continuum measured by *HST*/FOS (Meurer et al. 1995). Nevertheless, given the extent of both galaxies of the pair and the fact that *IRAS* observed the pair as a whole the $F_{\rm FIR}/F_{\rm UV}$ ratio is probably overestimated and has been flagged as an upper limit. Moreover since the *FUSE* aperture is centered on one galaxy of the pair, one must be cautious in comparing the observations of *FUSE*, *IRAS* and *HST*.
MRK59 is an HII region observed as a bright knot in the southern part of NGC 4861. Thuan et al. (2002) used the *FUSE* spectrum to study the heavy element abundance and the H_2 content of MRK59. Both *FUSE* and *IUE* apertures were centered on MRK59. The *IRAS* detection is also at the position of MRK59 but given its low resolution the FIR flux concerns NGC 4861. NGC 4861 has been observed in *UV* by the SCAP experiment at 2000 Å and its total flux is a factor of ~2 larger than that measured within the *IUE* aperture. The FIR to *UV* flux ratio is calculated with the total *UV* flux.

2.2. Data processing

All the fluxes were recorded with the LiF and SiC channels through the LWRS (30×30 arcsec^2) aperture. A summary of the observations is given in Table 2. Each observation consisted of several exposures. For the purpose of inter-comparison we report in Table 2 the signal to noise ratio for one spectral window used to measure the SED (window 4 at 1050 Å). The S/N values are rather low because of the small size of the window (9 Å).
The data were prepared for analysis by the *FUSE* data pipeline. Since the observations spanned 18 months, several versions of the pipeline were used to reduce the data. We compared the different versions of the pipeline to the last version (2.0.5) available at the time of writing this paper. The wavelength calibration has slightly changed; nevertheless since we are only concerned with the continuum, this change does not affect our results. We also observed a change in the absolute fluxes, especially between the earliest versions of the pipeline and the last one but once again this modification does not affect the shape of the continuum. Since we are only interested in relative fluxes we have not entirely re-processed the data with version 2.0.5 of the pipeline. For information, however, we list in Table 2 the approximative multiplicative factor to obtain absolute fluxes consistent with the last version of the pipeline.

We combined the individual exposures for each target weighted by the respective exposure times after checking that the mean fluxes and errors were consistent in the spectral windows of interest (see below for the definition of the windows). In a few cases some exposures were discarded because of discrepancies between the mean fluxes not consistent with the errors.

For each spectral window we then combined the two segments with the highest sensitivity weighted by their effective area taken from the *FUSE* observer's guide. Once again the combination was made after checking that the mean fluxes and errors were consistent in each individual segment: inconsistent data were discarded. In particular, the fluxes collected on the LiF2 channel were found to be lower than those obtained on the LiF1 channel for three targets (Tol1247-232, Tol1924-416 and MRK59). This effect is probably due to the target

Table 1. The sample of starburst galaxies with some useful characteristics. FIR fluxes at 60 and 100 μm ($F(60)$ and $F(100)$), galaxy sizes, Galactic extinctions and redshifts come from NED. The total observed *UV* flux at 1600 Å (Col. 7) and the slope β of the continuum ($F_\lambda = \lambda^\beta$) (Col. 4) come from various sources. a: Meurer et al. (1999); b: NED; c: Bell & Kennicutt (2001); d: Meurer et al. (1995) (the *UV* flux at 1600 Å is extrapolated from 2200 Å with the law $F_\lambda = \lambda^\beta$); e: Donas et al. (1987) (the *UV* flux at 1600 Å is extrapolated from 2000 Å with the law $F_\lambda = \lambda^\beta$); f: Kinney et al. (1993); g: Terlevich et al. (1993); h: Giavalisco et al. (1996). The observed *UV* fluxes were corrected for the Galactic extinction before the calculation of $F_{\rm FIR}/F(1600)$ (Col. 8). When the galaxy is very extended as compared to the *FUSE* aperture, $F_{\rm FIR}/F(1600)$ is flagged with an asterix. The metallicities (Col. 9) are taken from Heckman et al. (1998) except for few cases: Calzetti et al. (1994) for NGC 7673, Noeske et al. (2000) for MRK59, Terlevich et al. (1993) for Tol1247-232.

name	Size	$E(B-V)_{\rm G}$	β	$F(60)$	$F(100)$	$F(1600)$	log	Metallicity	redshift
	arcmin^2	mag		Jy	Jy	erg cm^{-2} s^{-1} Å^{-1}	$(F_{\rm FIR}/F(1600))$	$12 + \log$ (O/H)	z
NGC 1140	1.7×0.9	0.038	-1.78^a	3.36	4.92	4.2×10^{-14a}	<0.28	8.0	0.005
NGC 1705	1.9×1.4	0.008	-2.42^a	0.87	1.81	25.4×10^{-14b}	−0.93	8.0	0.002
NGC 3310	3.1×2.4	0.022	-1.05^a	34.13	47.95	52.2×10^{-14c}	0.24*	9.0	0.003
NGC 3504	2.7×2.1	0.027	-0.56^a	22.70	35.70			9.1	0.005
NGC 3690	1.2×1.0	0.017	-0.74^d	121.64	122.45	3.73×10^{-14d}	<1.9	8.8	0.010
NGC 5236	12.9×11.9	0.066	-0.83^a	266	639	233.3×10^{-14c}		9.3	0.002
NGC 7673	1.3×1.2	0.043	-1.50^a	4.91	6.89	7.5×10^{-14e}	0.19	8.5	0.011
NGC 7714	1.9×1.4	0.052	-1.23^a	10.52	11.66	3.3×10^{-14a}	<0.81	>8.7	0.009
MRK54	0.7×0.4	0.015	-1.78^a	0.93	1.83	1.7×10^{-14a}	0.25		0.045
MRK59	HII region	0.011	-2.57^f	1.97	2.46	19.9×10^{-14e}	−0.56*	8.0	0.003
Tol1247-232		0.089	-1.25^h	0.50		0.9×10^{-14g}	−0.03	8.1	0.048
Tol1924-416	0.8×0.4	0.087	-2.12^a	1.68	1.01	3.3×10^{-14a}	−0.18	8.1	0.010

Table 2. Summary of the observations. The factor listed in the last column is the mean ratio between the last absolute flux calibration (pipeline version 2.0.5) and the flux calibration effectively used to reduce the data, see text for details.

Target name	$T_{\rm exp}$ sec	S/N 1050 Å	pipeline version	factor
NGC 1140	4033	11	1.8.7	0.94
NGC 1705	7658	11	1.6.6	1.20
NGC 3310	27077	10	1.6.9	1.20
NGC 3504	13561	7	1.8.7	0.94
NGC 3690	15957	8.5	1.8.7	0.94
NGC 5236	26538	7.5	1.7.7	0.97
NGC 7673	10515	5.5	1.7.7	0.97
NGC 7714	5796	5.5	1.7.7	0.97
MRK54	27502	4	1.6.8	1.20
MRK59	9831	9	1.6.6	1.20
Tol1247-232	24303	5	1.6.9	1.20
Tol1924-416	5014	5.5	1.6.9	1.20

moving outside the LiF2 spectrograph aperture; in these cases we have only considered the LiF1 channel. We checked that the SiC channels were not affected by this effect.

We compared the fluxes measured by *FUSE* at 1180 Å with the spectra obtained by *IUE* longward of 1200 Å. The fluxes were consistent within 30%, which seemed reasonable given the different apertures (the fluxes are compared without any correction factor for the apertures) and the low sensitivity of *IUE* near 1200 Å. The only discrepant case was NGC 3690 for which *FUSE* observed a flux more than twice that measured by *IUE*. As discussed in the previous section, this discrepancy is likely to be due to the bad centering of *IUE*.

3. Deriving the spectral energy distributions

Our aim is to extract the spectral energy distribution from the very high resolution *FUSE* spectra. We have to get rid of the numerous absorption and emission lines from the Milky Way and the airglow. Given the low sensitivity at the shortest wavelengths and the presence of the Lyman series of HI we do not consider wavelengths shorter than 960 Å.

The adopted strategy is to define spectral windows avoiding Galactic and airglow lines: we are able to define 13 windows. They are described in Table 3. For the interstellar absorption lines we use the list of Barnsted et al. (2000). Two windows (3 and 4) contain weak Galactic interstellar lines (SiII 1020.7 Å and FeII 1055.5 Å); for each target we check that these lines are not present in the spectra. For the first window we use either window 1 or 1b according to the redshift of the target and the position of the lines. We have also to deal with potential absorption lines of Galactic molecular hydrogen along the line of sight. The windows that we define are taken as much as possible outside the Lyman and Werner bands of H_2. Nevertheless some lines remain. The contamination induced by this effect is estimated both with the *FUSE* simulator and with observed reference spectra (Shull et al. 2000) and does not exceed a few percents.

It is a much more difficult task to avoid the absorption lines in the objects themselves because their position varies with the redshift of the observed galaxy. Each target is analysed separately. If a window contains a line from the Lyman series of HI, it is suppressed. For the metal lines, if they are located at the edge of the window, we avoid them by redefining the limits of the window. For the lines located well within a window two cases are found: if the line is detected (or expected to be strong when the spectrum has a low S/N) the window is suppressed

Table 3. Spectral windows for the determination of the SED. Window 1 contains three segments 969–971, 974–976 and 979–981 Å. For each target we used either window 1 or window 1b according to the position of the absorption lines.

Num.	$\Delta\lambda$ Å	$\lambda_{\rm eff}$ Å	detector segment
1	969-971 974-976 979-981	975	SiC2A SiC1B
1b	967-971	969	SiC2A SiC1B
2	996-1001	999	SiC2A LiF1A
3	1016-1024	1020	LiF1A LiF2B
4	1052-1061	1057	LiF1A LiF2B
5	1068-1076	1072	LiF1A LiF2B
6	1087-1091	1089	LiF2A
7	1100-1107	1104	LiF2A LiF1B
8	1113-1120	1117	LiF2A LiF1B
9	1126-1130	1128	LiF2A LiF1B
10	1136-1143	1140	LiF2A LiF1B
11	1146-1152	1149	LiF2A LiF1B
12	1155-1167	1161	LiF2A LiF1B
13	1170-1175	1173	LiF2A LiF1B

or if the line is undetected (or expected to be weak when the spectrum has a low S/N) the window is kept.

The molecular hydrogen in the target may also cause some problems. Nevertheless, no H_2 is detected in the spectra of our galaxies, specifically the Lyman 4–0 and 3–0 bands are not detected even in the best spectra. Such an absence of H_2 lines was also reported for I Zw18 (Vidal-madjar et al. 2000) and two galaxies of our sample NGC 1705 (Heckman et al. 2001a) and MRK59 (Thuan et al. 2002). We assume that no H_2 lines contaminate the continuum of the galaxies even when the H_2 lines may not be detected because of a low S/N ratio.

The fluxes obtained in each spectral window are reported in Table 4. As discussed in Sect. 2.2 different versions of the *FUSE* pipeline were used to obtain these absolute fluxes. The mean factor to apply in order to obtain an absolute calibration consistent with the latest version of the pipeline (version 2.0.5) is given in Table 2. The errors quoted are estimated as the dispersion of the measurement within a spectral window (i.e. a combination of exposures and detector segments). It is checked that the error is always larger than the Poissonnian error calculated by the *FUSE* pipeline.

The SED of the galaxies, as defined by the fluxes in the spectral windows, are plotted in Fig. 1. The fluxes are corrected for the dust extinction inside our Galaxy. The color excess along the line of sight are from Schlegel et al. (1998). We adopt the extinction curve deduced by Sasseen et al. (2002). The color excess is low along the line of sight of the targets (cf. Table 1) and the correction is not large. We checked that the resulting SED are not sensitive to this correction by repeating the calculation using an extrapolation of the extinction curve of Cardelli et al. (1989) down to 900 Å. We report the observed wavelengths except for the two most distant galaxies (MRK54, Tol1247-232) for which rest frame wavelengths are considered.

4. Analysis of the far-UV spectral energy distributions

The first step to understand the basic features of the SED displayed in Fig. 1, a rather flat distribution from 1180 Å down to ∼1050 Å and a more or less pronounced decrease at wavelengths shortward of 1050 Å, is to compare them with the predictions of population synthesis. The Starburst99 models (Leitherer et al. 1999) are especially appropriate for this comparison and are presented in Fig. 2 at different steps in time. Figure 2 shows the rapid decline of the flux (especially at short wavelengths) for an instantaneous burst and the rapid equilibrium reached in the continuous star formation regime.

The four galaxies with a relatively flat SED (or slightly increasing at short wavelengths) in Fig. 1, NGC 1705, MRK59, Tol1924-416 and Tol1247-232 can be easily interpreted as a recent (age ≤ 10 Myrs) instantaneous starburst or a continuous star formation. The spectral shapes are the same because of the short time scale between star formation and star evolution off the domain of high effective temperatures. The lack (or small amount) of dust extinction is consistent with the low values of β for these objects (the case of Tol1247-232, $\beta = -1.2$, will be rediscussed later on).

The interpretation of the eight other objects is not as straightforward because the decrease of the flux at short wavelengths may result from one or a combination of two factors: an aging burst (or more complex star formation history) or dust extinction (in general reddening is known to increase at short wavelengths). The metallicity is known to be only a second-order effect and variations of the IMF within reasonable limits do not alter the spectral shapes. Although a separation of age and reddening is difficult, we present several arguments in the following for a dominant role of dust extinction.

1. The entrance aperture of *FUSE* is large enough to smooth the local variations of the star formation activity, which is likely to result in a continuous star formation. In such conditions, only dust extinction can produce the decrease of the flux observed at short wavelengths.
2. Some extinction is known to be present. Following Calzetti, Meurer and their collaborators the extinction of starburst galaxies at ∼1600 Å can be estimated from their $F_{\rm FIR}/F_{\rm UV}$ ratio or from the slope β of the *UV* continuum between 1250 and 2500 Å and defined as $F_{\rm lambda} \propto \lambda^{\beta}$ (e.g. Meurer et al. 1999; Calzetti et al. 2000). Using the empirical law of Calzetti et al. (2000)

   $$\mathrm{A}(1600\ \text{Å}) = 2.31\beta + 4.85$$

   leads to an extinction in the 12 objects that ranges from 0 to 2 mag.
3. We develop the previous argument and search whether the decline of the SED at short wavelengths is correlated with some tracers of the dust extinction. To this end we choose to quantify the decrease of the SED by averaging the fluxes measured shortward of 1050 Å in windows 2 and 3 (λ 1010 Å) and longward of 1050 Å in windows 4 to 6 (λ 1070 Å). The ratio of the averaged flux at long wavelengths over the averaged flux at short wavelengths will be

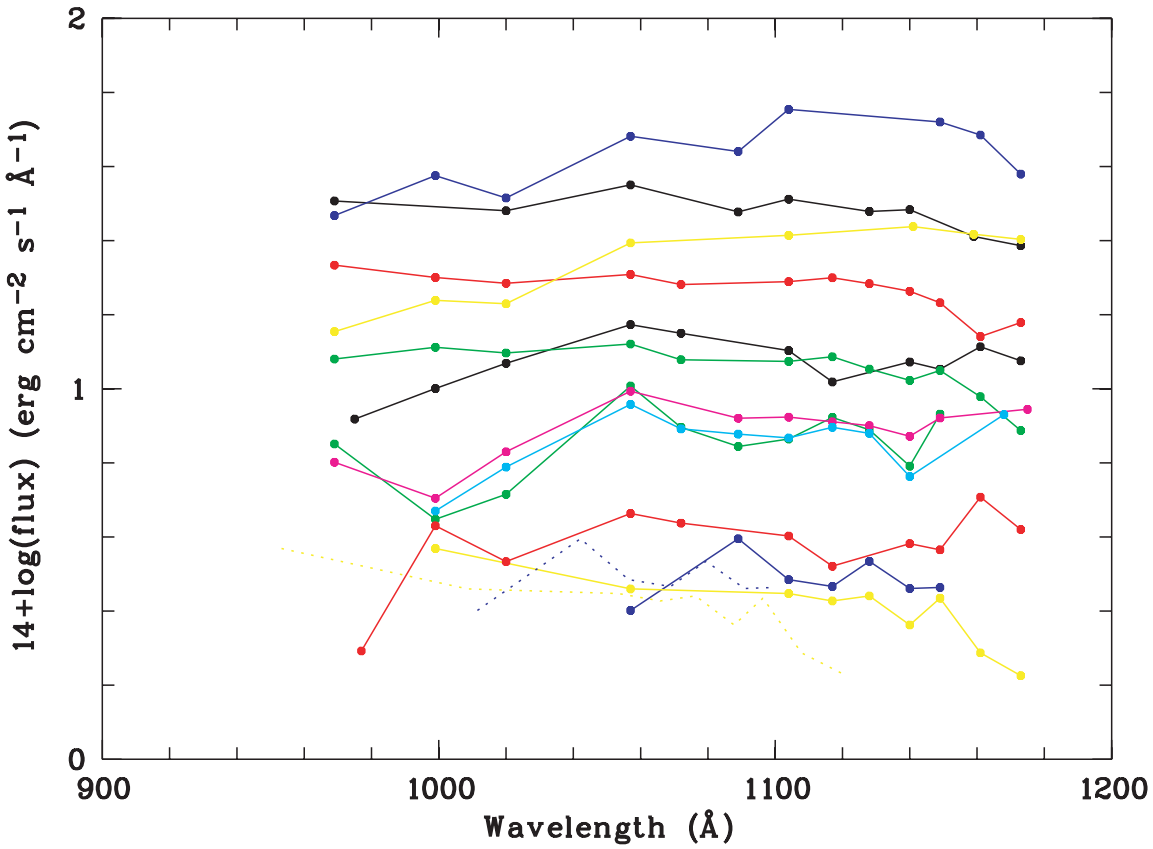

Fig. 1. FUV Spectral Energy Distributions. The fluxes were corrected for the Galactic extinction. By increasing flux at the largest observed wavelength: Tol1247-232 (yellow), MRK54 (blue), NGC 3504 (red), Tol1924-416 (green), NGC 7673 (cyan), NGC 7714 (magenta), NGC 3690 (green), NGC 1140 (black), MRK59 (red), NGC 1705 (black), NGC 3310 (yellow) and NGC 5236 (blue). For the two distant galaxies Tol1247-232 and MRK54, the rest-frame wavelength corrected distributions are plotted with dotted lines.

named R hereafter. The galaxies with a value of R close to unity have a flat spectrum.

We compare the values of R with $F_{\rm FIR}/F_{\rm UV}$, β (Fig. 3) and the metallicity of the galaxies (Fig. 4). In spite of the large error bars, there is an increase of R with $F_{\rm FIR}/F_{\rm UV}$; the trends are less pronounced but still present with 12 + log(O/H) and β. Both β and $F_{\rm FIR}/F_{\rm UV}$ are strongly correlated with 12 + log(O/H) (Heckman et al. 1998), all quantities being related to the amount of dust. Therefore the presence of dust extinction seems to be related to the decrease of the far *UV* SED downward 1050 Å.

4. In the absence of dust extinction, the interpretation of the decrease of the flux at short wavelengths would require an old starburst. In order to illustrate the comparison of the models and the data, we report in Fig. 4 the predictions of the Starburst99 models for R.

A constraint on the age of the stellar population may come from the analysis of spectral features present in the *UV* spectra. The *UV* absorption lines of NGC 1705, MRK59, NGC 3310 and NGC 5236 as observed by FUSE have already been discussed (Heckman et al. 2001a, 2001b; Thuan et al. 2002). We focus on the O VI λ1032 line since it is specifically studied by Gonzalez Delgado et al. (1997) as a star formation history indicator; the OVI, Lyβ and CII lines are also modeled with high spectral resolution in Starburst99. Since the analysis requires good S/N ratio spectra, we can add only NGC 1140 and NGC 3690 to the previously published cases listed above. Another limitation is the possible contribution of the interstellar medium into the formation of absorption lines, especially in starburst galaxies (e.g. Gonzalez Delgado et al. 1997).

OVI λ1032 is present in the spectra of all the galaxies except for NGC 3690 in which, unfortunately, an emission line of the airglow coincides with the OVI line. If the origin of this line is stellar, massive O stars must be present and this argues for the presence of a very young star population. In the case of NGC 3690 the shape of the Lyβ and CII lines is quite consistent with a constant star formation rate over some Myrs or an instantaneous starburst not older than 20 Myr. The case of NGC 3310 is puzzling since Leitherer et al. (2002) conclude to a lack of massive ionizing O stars from the HUT spectrum of the galaxy. One plausible explanation is that the FUSE and HUT apertures do not encompass the same regions of this large galaxy.

Therefore, the analysis of the OVI line supports a very recent star formation in these galaxies and makes an old starburst very unlikely to explain the decrease of the spectra.

Table 4. The observed Spectral Energy Distribution of the sample galaxies. The fluxes are in 10^{-14} erg cm^{-2} s^{-1} Å^{-1}. For each galaxy, the first line corresponds to the observed fluxes estimated in the spectral windows defined in Table 3, the second line is the error on the estimation of the flux. No Galactic extinction correction was applied. When the galaxy name has an asterix $*$ the first column corresponds to the wavelength 969 Å (spectral window 1b) instead of 975 Å (spectral window 1). The ratio R equal to F(1070 Å)/F(1010 Å) is listed in the last column together with its estimated error in the second line. Note that the fluxes were corrected for Galactic extinction before the calculation of R.

Galaxy	975*	999	1020	1057	1072	1089	1104	1117	1128	1140	1149	1161	1173	R
NGC 1140	4.9	6.1	7.3	9.6	9.2		8.4	7.0		8.0	7.7	8.9	8.2	1.3
	1.7	1.7	1.7	0.9	0.9		0.9	0.9		0.9	0.9	0.9	0.9	0.3
NGC 1705*	28.8		27.4	32.4		27.5	29.8		27.7	28.1		23.8	22.5	1.1
	3.0		3.0	3.0		3.0	3.0		3.0	3.0		3.0	3.0	0.2
NGC 3310	10.5	13.0	12.9	19.2			20.5			21.9		21.0	20.4	1.5
	3.0	3.0	3.0											0.3
NGC 3504	1.4	3.0	2.4	3.4	3.2		3.0	2.5		2.9	2.8	3.9	3.2	1.2
	0.7	0.7	0.5	0. 5	0.4		0.4	0.4		0.4	0.4	0.4	0.4	0.3
NGC 3690*	5.6	3.6	4.2	8.4	6.5	5.8	6.1	7.0	6.5	5.2	7.2	9.2	8.4	1.7
	1.3	1.3	1.3	1.0	1.0	1.0	1.0	1.0	1.0	1.0	1.0	1.0	1.0	0.6
NGC 5236*	11.7	15.9	14.4	22.4		21.2	28.0				27.0	25.1	19.9	1.3
	3.0	3.0	3.0	3.0										0.3
NGC 7673		2.7	3.6	5.5	4.8	4.7	4.7	5.0	4.9	3.7			5.6	1.5
		1.0	1.0	1.0	1.0	1.0	1.0	1.0	1.0	1.0			1.0	0.6
NGC 7714*	3.1	2.6	3.5	5.4		4.7	4.8	4.7	4.7	4.4	4.9		5.3	1.5
	1.1	1.1	0.8	0.8		0.8	0.8	0.9	0.8	0.8	0.9		0.8	0.6
MRK54				2.1		3.3	2.6	2.5	2.9	2.5	2.5			1.3
				0.5		0.3	0.3	0.3	0.3	0.3	0.3			0.3
MRK59*	18.5	17.3	16.8	17.9	16.9		17.3	17.8	17.2	16.4	15.3	12.4	13.6	1.0
														0.2
Tol1247-232		1.2		1.0			1.1	1.1	1.1	0.9	1.1	0.8	0.7	0.9
		0.5		0.2			0.3	0.3	0.3	0.3	0.3	0.3	0.3	0.2
Tol1924-416*	3.6	4.2	4.2	4.8	4.5		4.7	4.9	4.6	4.3	4.7	4.0	3.3	1.0
	1.3	1.0	1.0	0.9	0.9		0.9	0.9	0.9	0.9	0.9	0.9	0.9	0.3

5. We explore for all 12 galaxies how well the fluxes observed within each spectral window fit the models in terms of χ^2 minimization. We use the models displayed in Fig. 2 with a full set of metallicity, 12+log(O/H) = 8.93 (solar, Heckman et al. 1998), 9.23, 8.53, 8.23 and 7.62 in order to reproduce the range of metallicity of the targets (Table 1). We interpolate the results of the models given by Starburst99 to predict the fluxes within each spectral window defined in Table 3.
The 3 galaxies with a value of R close to unity (Tol1924-416, MRK59 and NGC 1705) are very well fitted with a constant star formation rate over 5 to 20 Myrs or very recent instantaneous bursts (1–10 Myrs) and a Salpeter IMF from 1 to 100 $M_\odot$. Indeed, to obtain a low value of R, the presence of very massive stars is necessary and an IMF deficient in massive stars (with $M_{\rm up}$ = 30 $M_\odot$) leads to too large values of R.
In contrast, for the galaxies exhibiting a larger value of R (i.e. a decrease of their spectrum at low wavelengths) the fits of the overall spectra with synthesis models are not good (reduced χ^2 always larger than 2) and reproduce only marginally the observed values of R. This poor fitting when only the stellar content is accounted for also argues for the role of the dust extinction in re-shaping the SED of the galaxies with a large R.

Before concluding this series of arguments, we come back to the intriguing case of Tol1247-232. This galaxy exhibits the lowest value of R and its flux downward of 1200 Å is continuously rising, the best fits are for a very recent burst (1 Myr) or a constant star formation over at most 5 Myrs. However, no model is able to reproduce the low value of R observed for this object although the large errors on the measurement of R prevent us from reaching any firm conclusions (Fig. 4). In any case, it is likely that its SED gives no room for a significant extinction. However this galaxy exhibits a rather high extinction estimated from its slope β (equal to -1.2): A(1600 Å) = 1.96 mag. The extinction is more moderate but still significant if we use the $F_{\rm FIR}/F_{\rm UV}$ ratio and again the calibration of Calzetti et al. (see below) with A(1600 Å) = 0.8 mag. The inconsistency between the evidence for dust and the blue spectrum appears in Fig. 3 where Tol1247-232 does not follow the general trends.

If we exclude the case of Tol1247-232, we reach the conclusion that the flat FUV SED of starburst galaxies are consistent with recent starburst or continuous star formation. The spectra that exhibit a decrease shortward of 1050 Å cannot be satisfactorily fitted by evolutionary models and require attenuation by dust for the presence of which we already have some evidence. In short, the differences between the relative spectral

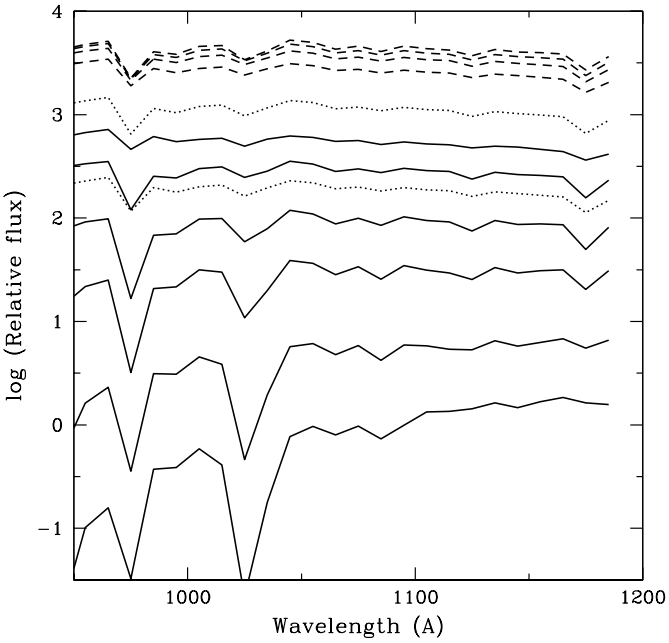

Fig. 2. The SED predicted in the far-*UV* by the population synthesis model Starburst99. Solid lines show the flux decrease of an instantaneous burst (1 $M_\odot$) observed after 1, 5, 10, 20, 50 and 100 Myrs. Dashed lines show a constant star formation rate (10^6 $M_\odot$ yr^{-1}) lasting (from bottom to top) 5, 10, 20 and 50 Myrs. A Salpeter IMF (slope −2.35) is adopted from 1 to 100 $M_\odot$ and the metallicity is solar. Dotted lines show the impact of a truncation of the IMF at 30 $M_\odot$ for the instantaneous burst of 1 Myr (bottom) and for the 5 Myrs continuous star formation (top). While the latter difference persists as a function of time (not shown for clarity), the impact becomes hardly noticeable for bursts older than a few Myrs; in both cases the relative spectral shape is not changed very much.

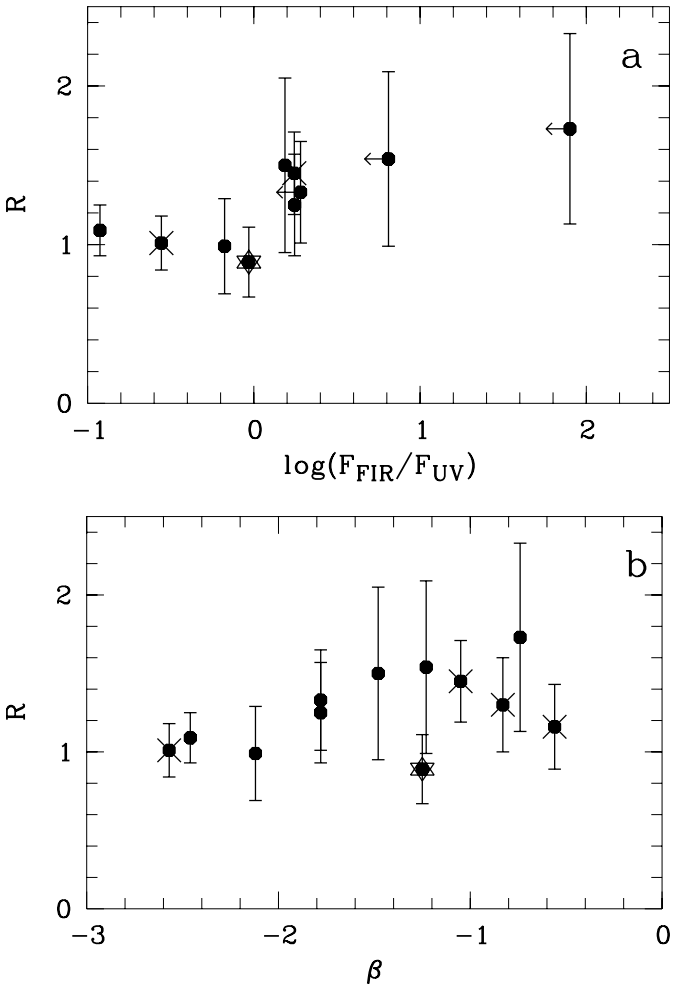

Fig. 3. $R = F(1070\ \text{Å})/F(1010\ \text{Å})$ plotted against $\log(F_{\rm FIR}/F_{\rm UV})$ **a)** and the slope β of the *UV* continuum **b)**. Extended galaxies for which *FUSE* and *IUE* data only concern the central part are plotted with crosses (NGC 3310, MrK59, NGC 3504 and NGC 5236). Tol1247-232 is plotted with a star.

energy distributions of our sample would be caused primarily by dust extinction.

5. The internal dust extinction

The obvious presence of dust in some of our targets allows us to study the properties of dust extinction in starburst galaxies in the far-*UV* (900–1200 Å). If our conclusion that the variations of spectral shapes are essentially due to dust extinction is correct, we can try to derive the attenuation law for starburst galaxies by comparing the spectra of dusty galaxies with a reference spectrum supposed to be without extinction. The method is similar to that used for the derivation of a stellar extinction law. Nevertheless in the case of galaxies the attenuation curve will be the result of the combined effects of dust properties and geometry (e.g. Calzetti et al. 1994; Leitherer et al. 2002).
We exclude from the analysis Tol1247-232 which has a spectrum bluer than any prediction of synthesis models. All the spectra are corrected for the Galactic extinction. The spectrum of each galaxy is rebinned according to the rest-frame wavelength from 965 Å to 1165 Å in bins of 25 Å. At this step, we discard MRK54 whose data only cover the rest frame spectral range from 1010 to 1100 Å.

Table 5. The dust-free reference SED normalized at 1140 Å, obtained by adding the spectra of NGC 1705, MRK59 and Tol1924-416.

965	990	1015	1040	1065	1090	1115	1140
1.14	1.11	1.07	1.15	1.12	1.07	1.08	1.0

In order to derive the attenuation curve we perform the following steps

1. We normalize all the observed spectra at 1140 Å.
2. We construct a reference spectrum without dust by adding the spectra of the 3 galaxies that exhibit a flat SED namely NGC 1705, Tol1924-416 and MRK59.
3. We assume that the departure of the other spectra from our reference spectrum is due to dust extinction alone and we deduce $A(\lambda) - A(1140\ \text{Å})$ for each galaxy.

The dust-free reference spectrum is given in Table 5. The resulting attenuation curves $A(\lambda) - A(1140\ \text{Å})$ for each galaxy are presented in Fig. 5. The normalization at 1140 Å is motivated by the lower dispersion found for the attenuation curve

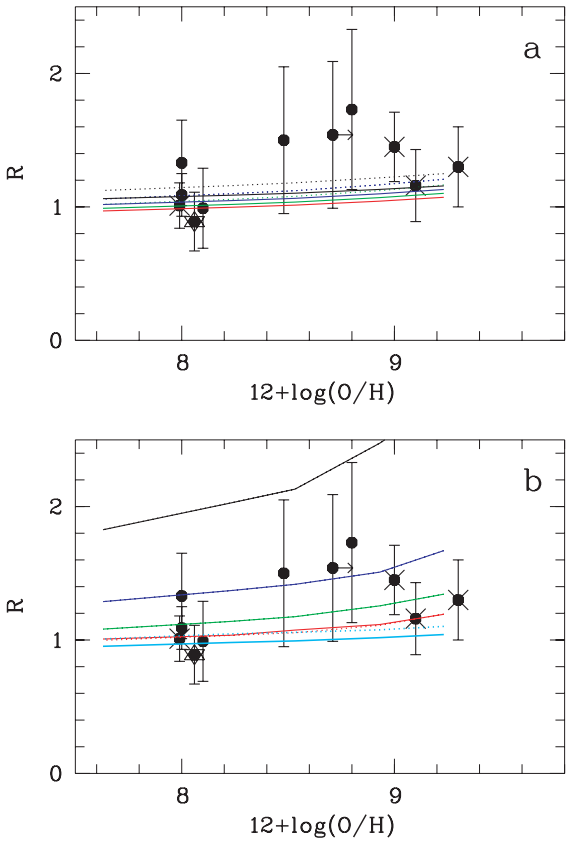

Fig. 4. $R = F(1070\ \text{Å})/F(1010\ \text{Å})$ plotted against the metallicity of the galaxies. The symbols are the same as in Fig. 3. The predictions of the models for **a)** a constant star formation over 5 (red), 10 (green), 20 (blue) and 50 (black) Myrs and **b)** 1 (cyan), 5 (red), 10 (green), 20 (blue) and 50 (black) Myrs after an instantaneous burst are overimposed. A Salpeter IMF has been adopted from 1 to 100 $M_\odot$) (solid line) or truncated at 30 $M_\odot$ (dashed line).

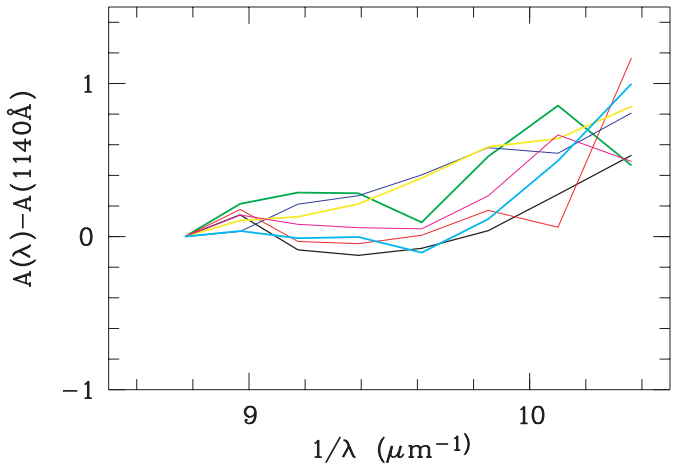

Fig. 5. The differential extinction $A(\lambda) - A(1140\ \text{Å})$ as a function of $1/\lambda$ in μm^{-1} for NGC 3504, NGC 7673, NGC 7714, NGC 3690, NGC 1140, NGC 3310 and NGC 5236. The colors used are the same as in Fig. 1.

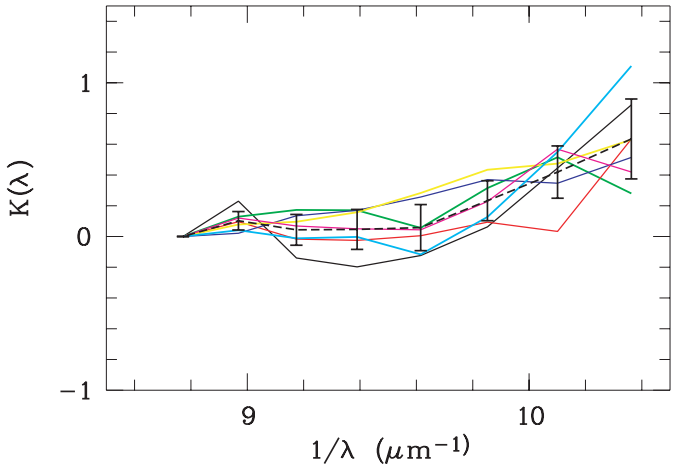

Fig. 6. The attenuation laws normalized at 1140 Å as a function of $1/\lambda$ in μm^{-1} for the same galaxies as in Fig. 5. The mean curve is drawn as a dashed line and the error bars indicate the standard deviation.

as compared to a normalization at 1165 Å. Moreover, the flux at 1165 Å (rest-frame) corresponds to an observed wavelength range where *FUSE* begins to be less sensitive.

Our approach is similar to that of Leitherer et al. (2002) but more empirical: they compared the observed spectra to model templates to derive the extinction curve whereas we prefer to construct empirically our reference spectrum with the galaxies exhibiting almost no extinction. Such an empirical approach was also adopted by Calzetti et al. (1994) to derive the extinction curve longward of 1200 Å.

In order to derive an attenuation law we need to normalize $A(\lambda) - A(1140\ \text{Å})$ by the amount of extinction for each target (equivalent to the color excess $E(B-V)$ used to normalize a stellar extinction law).
Quantifying the extinction in galaxies is a very difficult task. The slope β of the *UV* continuum longward of 1200 Å and the ratio $F_{\rm FIR}/F_{\rm UV}$ are expected to be quantitative tracers of the amount of extinction in starburst galaxies. Since the $F_{\rm FIR}/F_{\rm UV}$ ratio is only available for three targets (excluding the targets used to construct the reference spectrum) we adopt the slope β to normalize the dust attenuation law. Practically we follow the same method as Leitherer et al. (2002).

For each reddened galaxy we calculate:

$$k(\lambda) = \frac{A(\lambda) - A(1140\ \text{Å})}{\Delta\beta}$$

where $\Delta\beta$ is the difference between the observed slope β of the galaxy and the intrinsic slope of the reference spectrum $\beta_0 = -2.4$ (mean value for the three galaxies used to construct the reference spectrum).

The resulting attenuation laws normalized at 1140 Å are reported in Fig. 6. The average of the 7 curves gives the mean attenuation law $< k(\lambda) >$ and the standard deviation is taken as a measure of the error. The normalization only slightly decreases the dispersion between the curves which probably implies that the amount of extinction is not very accurately measured by $\Delta\beta$. Note however that our sample does not show a large range of extinction in terms of $\Delta\beta$. In the absence of another method to estimate the amount of extinction we continue with this normalization.

A polynomial fit of $< k(\lambda) >$ gives:

$$< k(\lambda) >= 32.356 - 7.1023/\lambda + 0.38995/\lambda^2$$

with λ expressed in μm.

In order to perform a comparison with other attenuation curves we also derive a more classical formula of the attenuation law related to the stellar color excess $E(B-V)_s$. To this end we need to relate $\Delta\beta$ and $A(1140$ Å$)$ to $E(B-V)_s$. We use the laws formulated by Calzetti et al. (2000) for starburst galaxies, extrapolated from 1200 to 1140 Å:

$$\Delta\beta = 4.72\ E(B-V)_s$$

and

$$A(1140\text{ Å}) = 12.75\ E(B-V)_s$$

and deduce

$$A(\lambda) = ((4.72\ \ < k(\lambda) > +12.75) \times E(B-V)_s$$

$$= (165.470 - 33.5229/\lambda + 1.84056/\lambda^2)\ E(B-V)_s$$

for the extinction of starburst galaxies between 0.095 and 0.1140 μm (λ is expressed in μm in the formula).

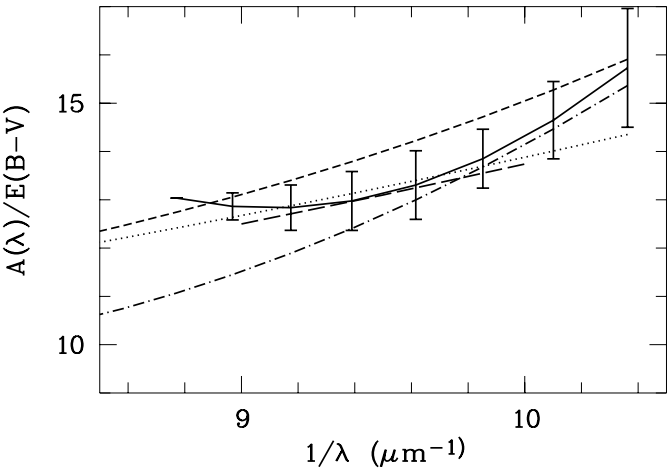

Fig. 7. Comparison between curves measuring the extinction in the far ultraviolet for galaxies and stars. The solid lines and the error bars refer to the attenuation curve derived in this paper. The dotted line is the attenuation curve of Leitherer et al. (2002); the short dashed line is the extrapolation of the attenuation law of Calzetti et al. (2000). The dot-dashed line is the stellar extinction curve of Sasseen et al. (2002). The long dashed line is the model of Witt and Gordon (2000) for a shell distribution, a clumpy dust and an optical depth in the V Band equal to 1.5.

6. Discussion

The attenuation curve obtained in the previous section is a mean curve and the estimated errors are rather large. As already discussed in the previous sections the far-*UV* SED of a star-forming galaxy is the result of the combined effects of star formation history, initial mass function and extinction. To deduce the attenuation curve we assumed that the departure of the observed SED from a template is entirely due to the internal dust extinction. The SED used as a dust-free template is consistent with a constant star formation rate over some Myrs.

We can try to test the validity of our approach a posteriori by applying our mean attenuation curve to the entire set of obscured spectra (the 7 spectra used to construct the attenuation curve and presented in Fig. 5) and perform again the analysis of Sect. 4 (points 3 to 5). All the corrected spectra exhibit a ratio R between 1 and 1.2 except NGC 3504 for which R is found equal to 0.8. Such values of R are consistent with a constant star formation or a very recent starburst (Fig. 4). We can also perform again the fit with synthesis models by a χ^2 minimization. However, one must note that the attenuation curve holds only in the range 950 to 1140 Å and leads to only 6 to 11 values per spectrum. In all cases the fitting procedure selects models with a recent star formation consistent with our dust-free template. The χ^2 values are lower than 1.5 for 5 of the 7 galaxies analysed. The two discrepant cases are NGC 3504 as expected from the value of its ratio R (0.8) and NGC 5236 (but for this object we have only 6 values for the SED). By comparison, the same procedure performed in Sect. 4 on the observed spectra of these 7 galaxies selected old starbursts with larger χ^2 values (>2) and did not reproduce correctly the values of R.

Therefore, the internal dust extinction is likely to be the dominant factor of the departure of the SEDs from the dust-free template. Nevertheless, whereas systematic effects are unlikely, we cannot exclude that the star formation history within each object has some (secondary) influence on the SED. This detailed star formation history combined with measurement errors and the uncertainty on the normalization of the attenuation law (cf. Sect. 5) can easily explain the dispersion found around the mean attenuation curve.

We can compare the attenuation curve derived with other curves measuring the extinction in the far ultraviolet. Very few such curves are available. Leitherer et al. (2002) deduced a mean attenuation curve from 900 to 1800 Å for ten star-forming galaxies with a method similar to ours. Because of its popularity we also extrapolated the law proposed by Calzetti et al. (2000) for starburst galaxies down to 965 Å ($10.34\ \mu m^{-1}$) even if it was not derived for this wavelength range. We also compare our attenuation curve to the stellar extinction curve obtained by Sasseen et al. (2002). The comparison between these curves is illustrated in Fig. 7.

The attenuation law derived in the present work is found almost flat from 8.8 to 9.6 μm^{-1} (1140 to 1040 Å) and rises at lower wavelengths. Given the error bars (only ours are reported) the various curves presented in Fig. 7 are consistent. Nevertheless, applying the attenuation law derived in this present work leads to a larger extinction than using that of Leitherer et al. (2002) for $\lambda \leq 1050$ Å. The difference in $A(\lambda)/E(B-V)$ reaches 1.4 units at 965 Å. In this wavelength range ($\lambda \leq 1050$ Å) our curve is very similar to the stellar extinction curve of Sasseen et al. (2002). Note that the extrapolation of the Calzetti et al. (2000) attenuation law gives a larger extinction than the other laws.

Witt & Gordon (2000) proposed several models of dust extinction in galaxies. The adopted geometry is spherical with a clumpy, dusty or shell distribution of the stars and the dust. In particular, they were able to reproduce the attenuation law of Calzetti (1997) assuming a shell distribution, a clumpy dust

medium and a mean optical depth in the V band equal to 1.5. Their predictions extend down to 1000 Å and we report them in Fig. 7. The model predicts a greyer extinction than our attenuation law, very consistent with the attenuation law of Leitherer et al. The model appears below the extrapolation of the law of Calzetti et al. (2000); this is likely to be due to the re-calibration of the attenuation law between 1997 and 2000, the model being adjusted to an older version of the attenuation law (Calzetti 1997).

7. Conclusion

We obtained the spectral energy distribution of 12 nearby starburst galaxies from 970 to 1175 Å. The high spectral resolution of *FUSE* allowed us to properly estimate the continuum out of the interstellar lines. The general behavior is a rather flat distribution, in general agreement with the predictions of population synthesis models in this wavelength range for active star formation. Nevertheless a decrease of the flux downward of 1050 Å is observed in some objects: the mean ratio of the fluxes at 1070 and 1010 Å is found to correlate with the metallicity and the extinction of the galaxies traced by their $F_{\rm FIR}/F_{\rm UV}$ ratio or the slope β of the spectral energy distribution longward of 1200 Å. The galaxies with an almost flat spectrum have almost no extinction and a sub-solar metallicity (0.1 to 0.2 $Z_\odot$); their spectrum is well fitted by a very young instantaneous burst of star formation or a constant star formation and a Salpeter IMF. The FUV spectra of the galaxies which exhibit a decrease of the flux below 1050 Å cannot be accurately fitted by any of the models we consider. These galaxies show evidence for dust extinction and have in general a metallicity from 0.4 $Z_\odot$ to 2 $Z_\odot$.

We deduce a relative dust attenuation law in the range 965–1140 Å by comparing the SED of the sample galaxies with a dust free template constructed with the SED of the galaxies that do not exhibit any trace of extinction. The total amount of extinction is measured with the observed slope of the *UV* continuum longward of 1200 Å. We also derive an attenuation law related to the stellar color excess $A(\lambda)/E(B-V)_{\rm s}$ by using (and slightly extrapolating) the calibrations of Calzetti et al. (2000). We give a simple polynomial parametrization of $A(\lambda)/E(B-V)_{\rm s}$. The extinction that we find is almost constant from 1165 to 1040 Å and rises at lower wavelengths. The agreement with the attenuation law proposed by Leitherer et al. (2002) is good at $\lambda > 1040$ Å but we find a larger extinction than Leitherer et al. at $\lambda < 1040$ Å. Nevertheless, given the error bars on both studies, the attenuation laws remain consistent.

Acknowledgements. This research is based on observations made with the NASA-CNES-CSA Far Ultraviolet Spectroscopic Explorer. FUSE is operated for NASA by the Johns Hopkins University under NASA contract NAS5-32985.

This research has also made use of the NASA/IPAC Extragalactic Database (NED) which is operated by the Jet Propulsion Laboratory, California Institute of Technology, under contract with the National Aeronautics and Space Administration.

References

Barnstedt, J., Gringel, W., Kappelmann, N., & Grewing, M. 2000, A&AS, 143, 193
Bell, E. F., & Kennicutt, R. C. 2001, ApJ, 548, 681
Cardelli, J. A., Clayton, G. C., & Mathis, J. S. 1989, ApJ, 430, 630
Calzetti, D., Kinney, A. L., & Storchi-Bergmann, T. 1994, ApJ, 429, 582
Calzetti, D. 1997, AJ, 113, 162
Calzetti, D., Armus, L., Bohlin, R. C., et al. 2000, ApJ, 533, 682
Deharveng, J. M., Sasseen, T. P., Buat, V., Bowyer, S., & Wu, X. 1994, A&A, 289, 71
Donas, J., Deharveng, J. M., Milliard, B., Laget, M., & Huguenin, D. 1987, A&A, 180, 12
Gonzalez Delgado, R., Leitherer, C., & Heckman, T. 1997, ApJ, 489, 601
Heckman, T. M., Robert, C., Leitherer, C., Garnett, D. R., & van der Rydt, F. 1998, ApJ, 503, 646
Heckman, T. M., Sembach, K. R., Meurer, G. R., et al. 2001, ApJ, 554, 1021
Heckman, T. M., Sembach, K. R., Meurer, G. R., et al. 2001, ApJ, 558, 56
Helou, G., Khan, I. R., Malek, L., & Boehmer, L. 1988, ApJS, 68, 151
Giavalisco, M., Koratkar, A., & Calzetti, D. 1996, ApJ, 466, 831
Kinney, A. L., Bohlin, R. C., Calzetti, D., Panagia, N., & Wyse, R. F. 1993, ApJS, 86, 5
Leitherer, C., & Heckman, T. M. 1995, ApJS, 96, 9
Leitherer, C., Schaerer, D., Goldader, J. D., et al. 1999, ApJS, 123, 3
Leitherer, C., Li, I.-H., Calzetti, D., & Heckman, T. M. 2002, ApJS, submitted
Meurer, G. R., Heckman, T. M., Leitherer, C., et al. 1995, AJ, 110, 2665
Meurer, G. R., Heckman, T. M., & Calzetti, D. 1999, ApJ, 521, 64
Milliard, B., Donas, J., Laget, M., & Huguenin, D. 1994, The balloon-borne 40-cm *UV* imaging telescope FOCA; results and perspective, 11th ESA Symp., Montreux
Noeske, K. G., Guseva, N. G., Fricke, K. J., et al. 2000, A&A, 361, 33
Sasseen, T. P., Hurwitz, M., Dixon, W. V., & Airieau, S. 2002, ApJ, 566, 267
Schlegel, D. J., Finkbeiner, D. P., & Davis, M. 1998, ApJ, 500, 525
Shull, J. M., Tumlinson, J., Jenkins, E. B., et al. 2000, ApJ, 538, L73
Stecher, T. P., Cornett, R. H., Greason, M. R., et al. 1997, PASP, 109, 584
Terlevich, E., Diaz, A., Terlevich, R., & Vargas, M. 1993, MNRAS, 260, 3
Thuan, T., Lecavelier des Etangs, A., & Izotov, Y. I. 2002, ApJ, 565, 941
Vidal-Madjar, A., Kunth, D., Lecavelier des Etangs, A., et al. 2000, ApJ, 538, L77
Witt, A. N., & Gordon, K. D. 2000, ApJ, 528, 799